Heterogeneous Scintillator Geometries to Maximise Energy Deposition for Waterborne Beta Particle Detection

Tilly Alton, t.alton@lancaster.ac.uk, Lancaster University

Dr Stephen Monk, s.monk@lancaster.ac.uk, Lancaster University

Dr David Cheneler, d.cheneler@lancaster.ac.uk, Lancaster University

Here the geometries that maximise detection efficiency of heterogeneous scintillators used to detect beta particles in aqueous solutions by maximising energy deposition are described. The determination of the geometry was achieved with the Monte Carlo code Geant4 using CaF_2:Eu scintillator as a pertinent case study, and validated with experimental data using single crystal CaF_2:Eu and heterogeneous CaF_2:Eu scintillators. Both 2D and 3D structures composed of arrays of primitive unit cells of packed spheres were examined to find the optimal geometry to maximise detection of volumetric sources of tritium and aqueous Carbon 14 and Lead 210. The 2D structures were evaluated relative to a single crystal scintillator and results show the detection efficiency of the 2D structures is maximised when the sphere radius is c.a. 0.46x the maximum track length of the beta particle in the scintillator. Data for the 3D structures show that the efficiency is maximised when the sphere radius is minimised, but it is further shown that practical issues limit the minimum radius that can be used for transient radiological contamination monitoring.

1. Introduction

Heterogeneous scintillators are multiphasic scintillators (Birks, 2013) that may consist of a porous structure whereby the scintillator is in the form of small particles instead of a single large crystal. The advantages of moving from scintillators in single crystal form to those made of an arrangement of small volumes have been examined before. The reason for the enhanced performance of nanoparticle scintillators was explored by Dujardin (Dujardin et al., 2010), who suggested that the crystal structure was altered by the particles small size which led to, for a number of reasons, a reduction in non-radiative recombinations, thereby increasing

luminescence. However, heterogeneous scintillators have the additional advantage of having a larger surface area than single crystal scintillators which helps mitigate attenuation effects of radiation monitoring in aqueous systems. For this reason, a number of heterogeneous scintillator flow cells have been devised (DeVol and Fjeld, 1995; Kawano et al., 2011; Shirahashi et al., 1984). In particular, Kawano et al. has recently published a number of papers based around a heterogeneous scintillator for tritium detection (Kawano et al., 2014; T. Kawano H. Ohashi and Jamsranjav, 2015).

A few studies have been conducted on the effects of the geometries of heterogeneous scintillators used for waterborne beta particle monitoring. For instance, Monte-Carlo modelling of heterogeneous scintillators was undertaken for 3D packed spherical geometries (Tan and DeVol, 2003). In that work, hexagonal close packed (HCP), face centered cubic packed (FCC), body centred cubic packed (BCC) and square packed (SP) spherical structures were analysed using the PENELOPE2000 Monte-Carlo code. While the simulations only considered initially mono-energetic low energy beta particles, they did show that porosity, material, sphere size and beta particle energy significantly affect detection efficiency. In particular, they showed that for low energies, smaller scintillator particle sizes increased the energy deposition within the scintillator and hence detection efficiency. Similarly, experimental results by Kawano et al. show that when using 25 µm, 50 µm and 150 µm radius 3D packed spheres, the smaller radius spheres results in more energy deposited in the scintillator as compared to in the water (Kawano et al., 2011).

An area currently unexplored is the use of 2D heterogeneous scintillators. It will be shown here that there are practical advantages to using 2D structures for transient environmental monitoring of radiological contamination of aqueous systems. This paper also uses Monte-Carlo combined with flow cell analysis to examine both 2D and 3D packed spherical structures with a view of maximising the energy deposition into the scintillator. The majority of this article will focus on tritium because of its detection challenges (Alton et al., 2017); however, both aqueous Carbon 14 and Lead 210 will also be analysed as they are common tracers in the environmental sciences, and the results show the conclusions derived are quite general.

Europium activated Calcium Fluoride (CaF_2:Eu) is used as the scintillator material throughout this work. This is because CaF_2:Eu is an ideal scintillator for flow cell based detectors due to its non-hygroscopic nature, its refractive index similar to that of Silicon Photomultipliers (SiPM), an emission curve that aligns with the peak efficiency of SiPMs (Materials, 2017; Sensl, 2017) and a similar output brightness (30,000 photons per MeV)

when compared with the commonly used NaI:Tl (Gobain, 2017; Materials, 2017). The inorganic scintillator can also be formed into a heterogeneous scintillator as particulate CaF_2:Eu with varying sphericity has been fabricated through various chemical approaches (Ritter et al., 2014). It is therefore particularly suitable to be used to detect tritium, commonly found in the form of tritiated water in the environment, whereby it replaces the ^{1}H in H_2O with ^{3}H and decays with a low energy beta particle (<18.6 keV) with a half-life of 12.3 years. The current standard for detecting tritiated water is liquid scintillation counting due to its high efficiency (Elmer, 2017), while single crystal designs suffer from very low efficiency (Alton et al., 2017). However, liquid scintillation is inconvenient for transient monitoring of radiological contamination. Heterogeneous flow cell scintillator detectors have been developed as a compromise between liquid scintillation and single crystal scintillation. This work shows that the efficiency of these heterogeneous detectors can be maximised with appropriate scintillator geometry choice.

2. Method

2.1 Geant4

The simulations for this article were carried out using the Geant4 10.3 (INCERTI et al., 2010; J Allison et al., 2006) Monte Carlo software. Geant4 is a library of tools for the simulation of nuclear and particle physics and is freely available, its applications range from nuclear reactor physics and high energy particle physics to radiotherapy and shielding. Some advantages of the Geant4 software is the flexibility of the code allowing the user to tailor each simulation to the application, improving the efficiency of the simulation and only analysing the relevant parts. The Geant4 physics packages used in the following simulations included the standard electromagnetic (EM) processes, with the eIonisation and eBremsstrahlung functions, electron ionisation and bremsstrahlung respectively. These two used the Livermore models for improved accuracy at low energies.

2D heterogeneous scintillators were modelled as planar arrays of face-centered-cubic (FCC) and square packed (SP) spheres (see Fig. 1). As is experimentally relevant, the arrays of spheres were modelled as being supported beneath by a thick layer of polydimethylsiloxane (PDMS) and exposed to a thick layer of radiologically contaminated water on top. The water acted as a source of tritium, aqueous carbon 14 and lead 210 in turn, modelled as cubic volumes of water with homogeneously distributed isotropic beta sources. The energies of

the beta particles were described through a 1000 bin histogram, with 10^8 beta particles and using radiological data for each isotope from the Radiological Toolbox (Center for Radiation Protection Knowledge, 2015). In order to create accurate models in the simulations any beta particles generated in the scintillator material in the simulations were immediately killed as the initial position of the beta particle should be within the water. In addition generated photons were not tracked, as photon detection is outside the scope of this work and is assumed ideal. These geometries were compared to an equivalent sized single crystal CaF_2:Eu scintillator. The thicknesses of the PDMS and water layers were set to exceed the maximum beta particle track length and can be assumed to be effectively infinite in depth; the values are shown in Table 1. The actual simulations were formed from arrays of the unit cells described in Fig. 1 tiled together. For the square packed array, the lateral dimensions of the unit cell were 2x the scintillator particle radius, i.e. $2R$. The lateral dimensions of the face centred cubic unit cell were $4Rsin(45°)$. Convergence studies showed that arrays of 1000x1000 tiled unit cells were equivalent to infinite 2D surfaces, i.e. edge effects were negligible. These structures are named *2D* as the position of each sphere can be described in $\hat{x}$ & $\hat{y}$ coordinates. A development of this utilises a dual 2D layer design whereby two 2D spherical packed planes with an optimal 3.5 μm radius SP arrangement are placed facing each other to act as a channel. Here, the water source is placed between the two layers and simulations were ran to determine the efficiency of the flow channel as a function of width, i.e. the gap between the two layers. The intent is that this structure can be layered to create a quasi-3D structure with practical advantages over a homogeneous 3D packed spherical structure.
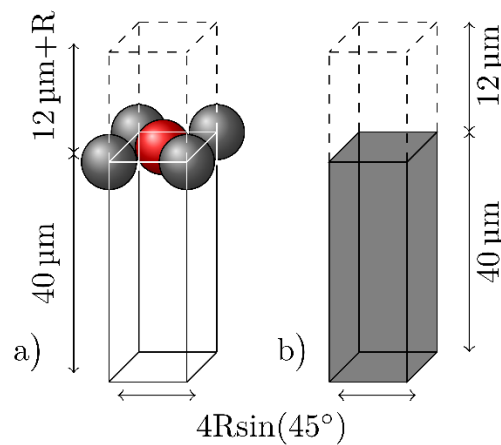
Isotope	Single Crystal Water (Dashed Volume) Height	Single Crystal Scintillator Height	Microparticle Water (Dashed Volume) Height	Microparticle Substrate Height
Tritium	12µm	40µm	12µm+R	40µm
Carbon 14	0.6mm	1.2mm	0.6mm+R	1.2mm
Lead 210	150µm	300µm	150µm+R	300µm

Table 1: Thickness of the various layers for the 2D unit cells for the Geant4 simulations. Where R is the radius. See Fig.1 for the schematic of these geometries.

3D heterogeneous scintillators were modelled as face centred cubic, body centred cubic and square packed arrays of spheres (see Fig. 2). As before, these spheres were comprised of CaF_2:Eu scintillating material and interspersed with radiologically contaminated water as described above. The lateral size of these unit cells were same as the 2D structures, with the equivalent height. The body centred cubic unit cell has dimensions of $4R/\sqrt{3}$. These unit cells were tiled in the three Cartesian directions so the simulations consisted of 1000x1000x1000 unit cells which behaved effectively as an infinite array, which is again backed up by convergence studies. These structures are labelled as 3D as the position of the spheres can be described in $\hat{x}, \hat{y}$ & $\hat{z}$ coordinates. The results shown in Figs. 5 & 6 are made from repeated simulation runs, each with a fixed radius.
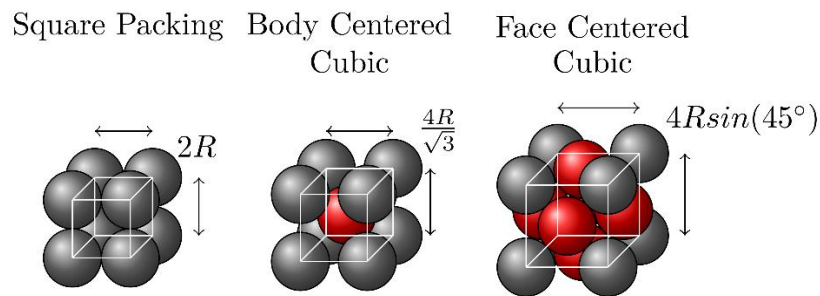
Figure 2: Diagram of the 3D structures for the Geant4 simulations. Red and grey colours indicate the scintillator material. The white box shows the unit cell with the dimensions shown for each unit cell.

The efficiency of the heterogeneous detector was defined as the ratio of the energy deposited by a beta particle in the scintillator material divided by the sum of the initial beta particle energy. The error for each value is calculated as the variance using the Welford method (Chan and Golub, 1983; Welford, 1962). For determining the track lengths and geometrical track lengths, an additional simulation using a beam source of each radionuclide in a 2m^3 cubic body of water was used with 10^9 per radionuclide. Here the track length is defined as the sum of the distances between each step, correcting for multiple scattering, while the geometrical track length is defined as the sum of the distances between each step along the axis of the beam.

2.2 Experimental Detector

Two scintillators were compared for the experiments, both using CaF_2:Eu from Hellma-Materials; a cylindrical single crystal (15 mm radius, 2 mm thickness) and a 2D heterogeneous scintillator. To make the heterogeneous scintillator, single crystals of CaF_2:Eu were crushed to size using a mortar and pestle. The particle size and distribution was measured by dispersing in de-ionised water (using a MasterSizer 3000 instrument, see Fig.3 for the results) and images taken with an optical microscope using the bright field. In Fig. 3, it can be seen the mean and max particle sizes are c.a. 1 µm and 8.8 µm respectively, comparable to the track length of tritium. The substrate for the particles was made from PDMS using the Dow Corning two-part mix kit (Corning, 2017) at a ratio of 10:1. It was partially cured for 22 hours at room temperature before the microparticles were evenly distributed on its surface, then left to fully cure at room temperature. An image of the cured PDMS with CaF_2:Eu embedded is shown in Figs.4 & 5.
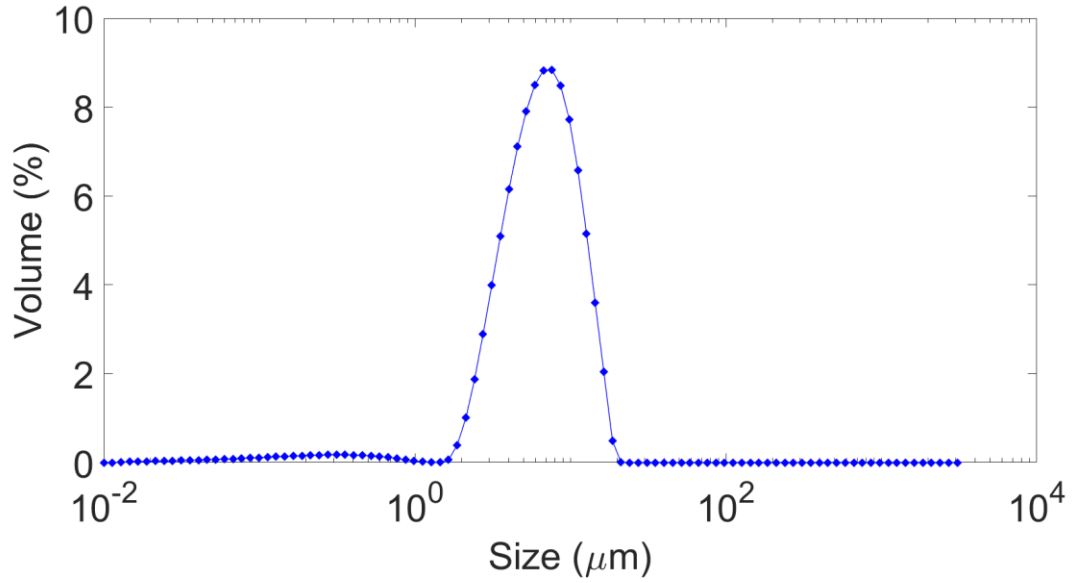
Figure 3: Histogram showing the size distribution of the heterogeneous scintillator produced by mortar & pestle from a single crystal. This is an average result of three measurements.

These scintillators were integrated onto a single 6x6 mm SiPM C series from Sensl which was interrogated with a transimpedance preamplifier (time constant = 20 μs) and a National Instruments ADC (400 KS/s and 16 bit resolution). All experiments were undertaken within in a light-proof box. The detectors were exposed to static volumes of tritiated water, approximately 20 mL with a concentration of 1,500 Bq/mL and deionised water which acted as a control for background count experiments. In both cases, the detectors were monitored for 30 minutes. Sealed point sources of Pb 210/Bi 210 and Cl 36 were used to calibrate the detector. The data was analysed using a LabView peak detection code with a threshold at 80 mV. The error for the experimental data was expressed as $\partial S = \sqrt{S}$ & $\partial B = \sqrt{B}$ for the raw and background data respectively. The error of the subtraction of them is then $\partial T = \sqrt{(\partial S)^2 + (\partial B)^2}$.
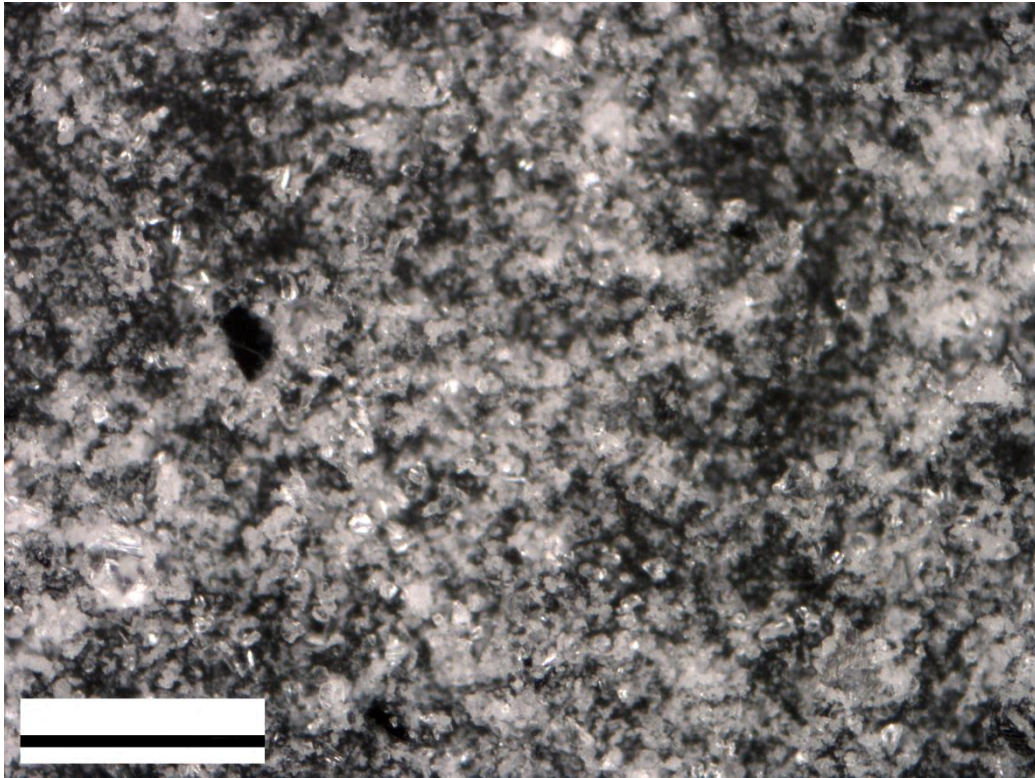
Figure 4: Optical microscope bright field image of the surface of the particulate heterogeneous scintillator taken at 5x magnification. The scintillator chosen is CaF$_2$:Eu with PDMS as the substrate. The scale bar in the corner equates to 200 μm in length.
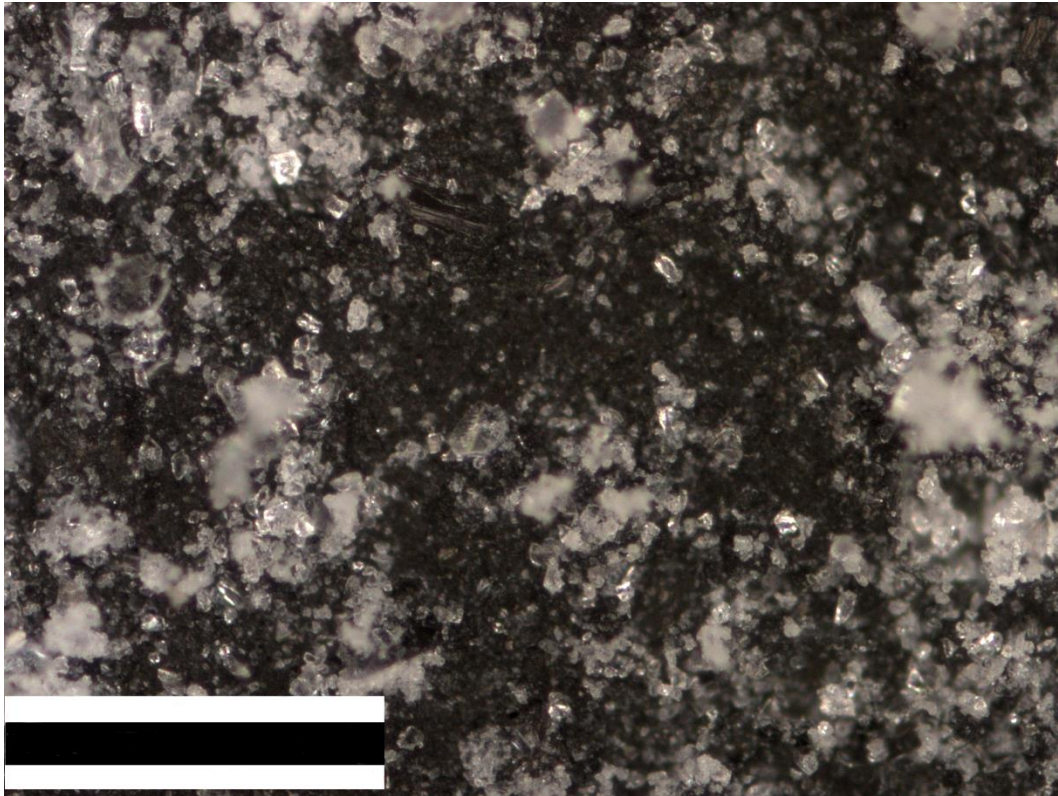
Figure 5: Optical microscope bright field image of the surface of the particulate heterogeneous scintillator taken at 10x magnification. The scintillator chosen is CaF_2:Eu with PDMS as the substrate. The scale bar in the corner equates to 300 μm in length.

3. Results & Discussion

3.1 Geant4

The simulation investigating the maximum track length and maximum geometrical track length in water

produced the results shown in Table 2.

Isotope	Maximum Track Length (μm)	Maximum Geometric Track Length (μm)
Tritium	7.541	4.088
Carbon 14	340.004	201.724
Lead 210	63.544	35.553

Table 2: Table showing the Maximum Track Lengths and Maximum Geometric Track Lengths for tritium, carbon 14 & lead

210. Here the Maximum Track Length is the maximum distance the beta particle travelled calculated by summing the

distances between each scattering event and the Maximum Geometric Track Length is the maximum straight-line distance

travelled from point of origin to final particle location. These results are from Geant4 simulations.

The results for the 2D structures are shown in Fig.6 and these show that for all three radionuclides there exists a peak that achieves an approximate 20% improvement in energy deposited in the 2D heterogeneous scintillator over a single crystal scintillator. The results for the single crystal show the expected constant efficiency. The X axis in the data is the Radius, if this is normalised by the Maximum Track Length values the peaks in the single crystal data align at a value of 0.46 Radius/Maximum Track Length. The same normalising technique also works when using the Maximum Geometric Track Length values instead, using Table.2. Then the peak in the single crystal data is located at 0.81 Radius/Maximum Geometric Track Length. The peaks in the data sets shown highlight the potential performance benefit by replacing a single crystal inorganic scintillator with a layer of small particles. The normalisation process stated above could be used to arrive at a general conclusion for beta decaying radioisotopes, if the maximum track length or maximum geometric track length be known the radius associated can be calculated.

Fig.7 shows the 3D structure results; here energy deposition into the scintillator is increased with decreasing scintillator particle radius. It should be noted that if normalised using the Maximum Track Length and Maximum Geometrical Track Length the tritium and carbon 14 data overlay one another suggesting a general result, however the lead 210 results do not align quite as well but are certainly comparable. The absolute efficiency calculated from the simulation for the 2D structures is dependent on the height of the source and water, therefore the absolute efficiency is not an objective result, unlike the 3D structures, however the relative efficiency, i.e. efficiency as compared to the single crystal results exposed to the same volume, is. These results are in agreement with previous research (Tan and DeVol, 2003), however the normalisation method used for the 2D structures in Fig.6 doesn't work here as is shown by the lead 210 curve.

The results from the dual 2D layer of microparticles are shown in Fig.8, highlight that with the gap between the layers decreasing the energy deposited increases. As the results show that by comparison with a single layer the dual 2D layers has a further increase in energy deposition. Then this model could be used as the basis of a flow cell detector, in which tritiated water flows between thin closely spaced layers, which would have beneficial flow and flow cell management properties. It has been shown that a 2D heterogeneous spherical packed layer is more efficient than a single crystal scintillator. As a single crystal can be crushed down to produce the particles, then a spherical packed layer can be formed with a larger surface area for the same volume of scintillator, which corresponds to a cost saving. Simple numerical calculations can reveal the

increase in surface area by crushing a single crystal down to produce a thin layer of micro particles. If the single crystal is assumed to be of radius 5 mm and thickness 2 mm (i.e. initial surface area c.a. 0.79 cm^2), then Table 3 contains the calculated surface area of the single layer of micro particles. Here the particulate surface is assumed to be square packed with a constant radius, the radius assumed for each is listed in the table.

Isotope	Particle Radius (μm)	Surface Area (cm^2)
Tritium	3.5	428.49
Carbon 14	150	9.99
Lead 210	30	49.98

Table 3: Numerical calculations to determine the surface area of a crushed single crystal producing a layer of square packed particles of uniform radius.
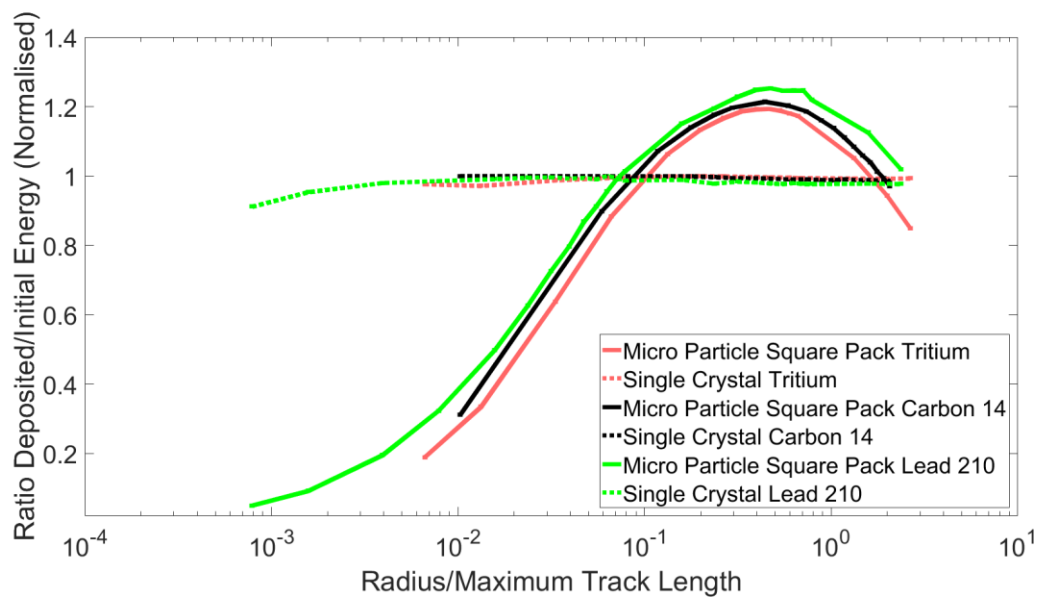

Figure 6: Results for the 2D arrangements from the Geant4 simulations. Face centered cubic arrangements were ran and the results overlay with the Square Packed and therefore have not been plotted. Plotted error bars are of small magnitude.
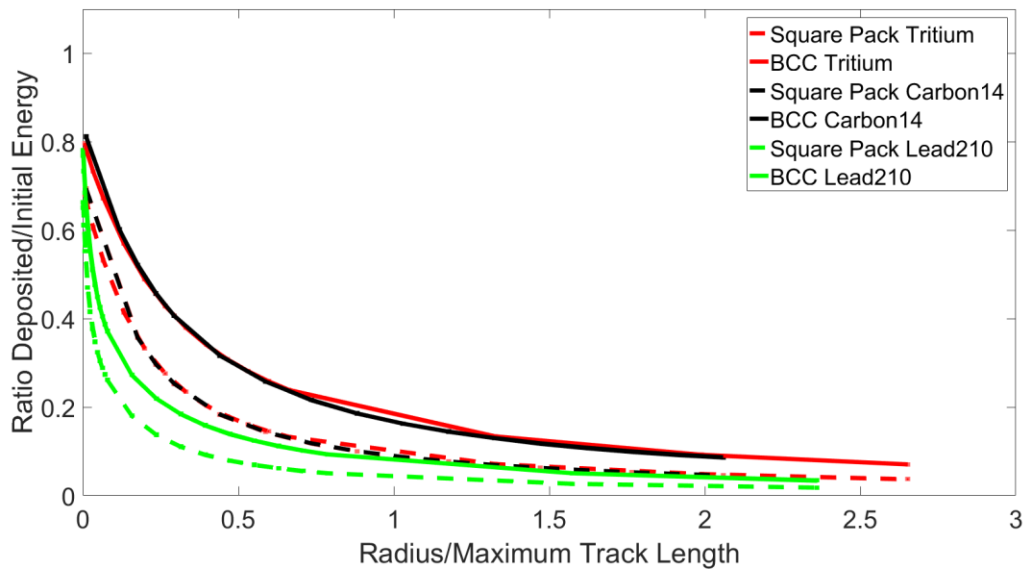
Figure 7: The results of the 3D arrangements for tritium, carbon 14 and lead 210 from Geant4. Face centred cubic arrangements were ran and the results overlaid with the Square Packing and therefore were not plotted. Error bars are plotted but of small magnitude.
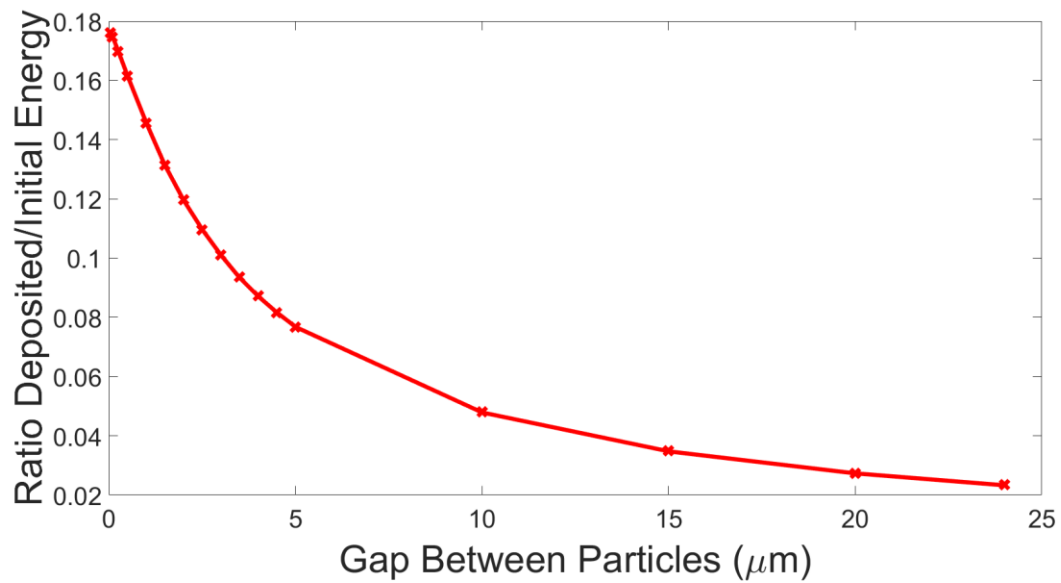

Figure 8: Results from a Geant4 simulation showing the efficiency of two layers of heterogeneous scintillator particles with increasing distance between the layers of particles. The isotope used was tritium and the radius fixed at 3.5 μm with an SP arrangement.

3.2 Experimental Validation

The data from the experimental detection setup comparing the single crystal to a 2D heterogeneous scintillator is shown in Table.4. Here a source of tritiated water of 1500 Bq/mL is compared with DI water for both scintillator designs.

Count Time (s)	Single Crystal Scintillator Total Counts	Prediction using the Single Crystal Scintillator	2D Heterogeneous Scintillator Total Counts
600	151393+/-406	181670+/-487	173421+/-228
1200	293481+/-568	352180+/-681	339450+/-305

Table 4: The results of the experimental setup of the single crystal scintillator and a comparable heterogeneous scintillator. Shown is the total counts i.e. those from tritium minus those from background. The prediction is taken to be a 20% increase of the single crystal with associated error.

The experimental data shows that the heterogeneous scintillator has resulted in an increase of the total counts by 15%. An increase in the energy being deposited into the scintillator will increase the pulse amplitude making detection above noise more likely, although this isn't the predicted 20% improvement there is still an increase validating the Geant4 results.

3.3 Practical Considerations

Consider the scenario in Fig.9, whereby a detector comprised of a porous heterogeneous scintillator is being used to monitor the concentration of beta particle emitting radionuclides in an open channel, such as a river. At some past time, contaminated water was released into the channel. This contaminated water contains a concentration, C_0, of a beta particle emitting radionuclide such as tritium. The contamination is assumed to flow as a plug of width, w, at a velocity, v. Note that this neglects issues such as dispersion, evaporation, decay etc. but the conclusions apply quite generally.
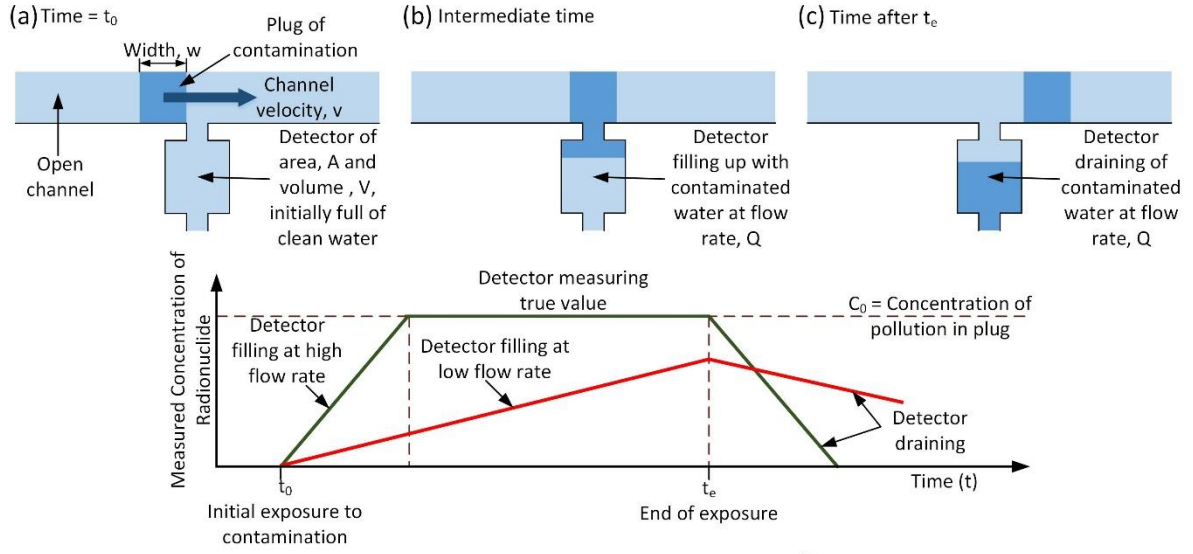
Figure 9: Top row depicts schematics of the fill level of a porous scintillator-based detector at various times, i.e. (a) before exposure, (b) during exposure where the detector is filling up with contaminated water and (c) after exposure where the detector is draining but still contains contaminated water. Bottom figure shows the effective concentration as measured by the detector at different times assuming both high and low flow rates though the detector.

Naturally, what is desired is for the detector to measure the true concentration of the contaminated water. However, the detector is only exposed to the contamination for a finite time, $T_e = t_e - t_0 = w/v$ (assuming the length/diameter of inlets to be negligible) and the detector takes a finite time to fill, $t_f = V/Q$, where Q is the flow rate through the porous scintillator, see Fig.9. If the flow rate into the flow cell is too slow, then it is possible that the detector may never read the true concentration of the contamination. This may be the case for 3D packed structures comprised of very small particles. The volume of contaminated water in the detector at a given time is:

$$V_t(t) = \begin{cases} if \ t_f > T_e \quad Q.(t - t_0) \quad for \ t_0 < t \le t_e \\ otherwise \quad Q.(t - t_0) \quad for \ t_0 < t \le t_f \\ \qquad\qquad V \quad for \ (t_0 + t_f) < t \le t_e \\ V_t(t_e) - Q.(t - t_e) \quad for \ t > t_e \\ 0 \quad for \ t < t_0 \ and \ t > (t_e + t_f) \end{cases}$$

The flow rate through the porous scintillator is given by the Carman-Kozeny equation (Carman, 1937; McCabe et al., 2005):

$$\frac{dp}{dx} = -\frac{150\mu}{\Phi^2 D_p^2} \frac{(1 - \epsilon)^2}{\epsilon^3} u \qquad (5)$$

where dp/dx and u is the pressure gradient and mean flow velocity through the porous scintillator respectively, µ is the viscosity of the fluid, taken here to be effectively water so that µ = 1.002 mPa/s, ε is the scintillator porosity (ε = 0.476 for cubic packed spheres), Φ is the sphericity which equals 1 and D_p is the mean scintillator particle diameter.

If C_0 [mol/L] is the concentration of the radionuclide in the contaminated water and the specific radioactivity is (Knoll 2010):

$$a[Bq/g] = \frac{1.32 \times 10^{16}[mol^{-1}]}{T_{1/2}[year] \times m[g\ mol^{-1}]} \qquad (6)$$

where $T_{1/2}$ is the half-life of the radionuclide and m is its mass number, the activity measured by the detector as a function of time is:

$$A[Bq] = V_t(t)[L] \times C_0[mol\ L^{-1}] \times m[g\ mol^{-1}] \times a[Bq/g] \qquad (7)$$

As an example, consider a river following at 1 m/s contaminated by 0.1 nM of tritiated water such that it forms a plug 100 m long (exposure time of T_e = 100 s). The mass number and half-life of tritiated water is 22.0315 g/mol and 12.3 years respectively and so it has a specific activity of 4.87x10^{13} Bq/g. At this concentration, the activity per volume will be 107.3 kBq/L, which is at dangerous levels. Let the scintillator be 100 mm x 100 mm x 100 mm (V = 1 L) in size and comprised of cubic packed spherical particles of diameter 10 µm so that the maximum water volume in the scintillator is $\varepsilon.V$ = 0.476 L. Let the pump apply 10 kPa across the scintillator (a low pressure as not to cause loss of the scintillator material). In this case, by rearranging eq.5, the flow velocity through the scintillator can be found to be:

$$u = -\frac{dp}{dx}\frac{D_p^2\varepsilon^3}{150\mu(1-\varepsilon)^2} = 2.94 \times 10^{-5}\frac{m}{s}$$

Multiplying this velocity by the cross-sectional area of the scintillator gives the flow rate. In this case Q = 0.29 mL/s and so filling time, t_f = 1618 s. The filling of the flow cell and the monitoring of the activity within the flow cell will be continuous and simultaneous, as the experimenter will not know when the contamination will reach and leave the flow cell. In this scenario, the detector never completely fills up with contaminated water and so the maximum measured count rate would be 3.16 kcps (1.62 kcps average counts over $t_0 < t < t_0 +$

$t_e + V_t(t_e)/Q$) while the maximum possible expected total counts would be 51.08 kcps (neglecting detection

inefficiencies and attenuation effects). Therefore, to the experimenter, the contamination would appear to

have a triangular profile over 200 s with an average and peak concentration of 3.17 pM and 6.19 pM

respectively, far from the constant 0.1 nM concentration for 100 s that is expected. However, if the scintillator

particles had a mean diameter of 100 μm the fill time would be much reduced (t_f = 16.2 s) so it would be

completely filled by contaminated water. Therefore, the maximum possible measured count rate would be

51.08 kcps as expected with an average count rate of 46.68 kcps. The experimenter would therefore see a near

constant contamination concentration of 0.1 nM for 80 s with an average of 0.091 nM over 120 s which is

much closer to the actual value.

This shows that while 3D packed sphere based flow cells become more efficient as the particles get smaller

(see Fig.7) in terms of reducing attenuation effects, they becomes less effective at capturing transient activity

levels owing to the reduced permeability. A pseudo-efficiency or a measure of flow cell efficiency can be

deduced by multiplying element wise the maximum flow rate (which is proportional to the permeability) and

the scintillator energy deposition. In this way, it becomes possible to determine the ideal particle size. The

energy deposition/initial ratio, flow rate and aforementioned optimal are plotted in Fig.10. For maximum

clarity, both the flow rate and energy ratio were normalised by first subtracting the minimum of the data set

then dividing by the range. This data shows that the efficiency gives an optimal peak. Table 4 shows the radius

for each radionuclide corresponding to the optimal peak.

Isotope	Optimal Radius (μm)
Tritium	10
Carbon 14	350
Lead 210	75

Table 5: Optimal radius corresponding to the optimal peak shown in Fig.10. The peak radius value is remains the same
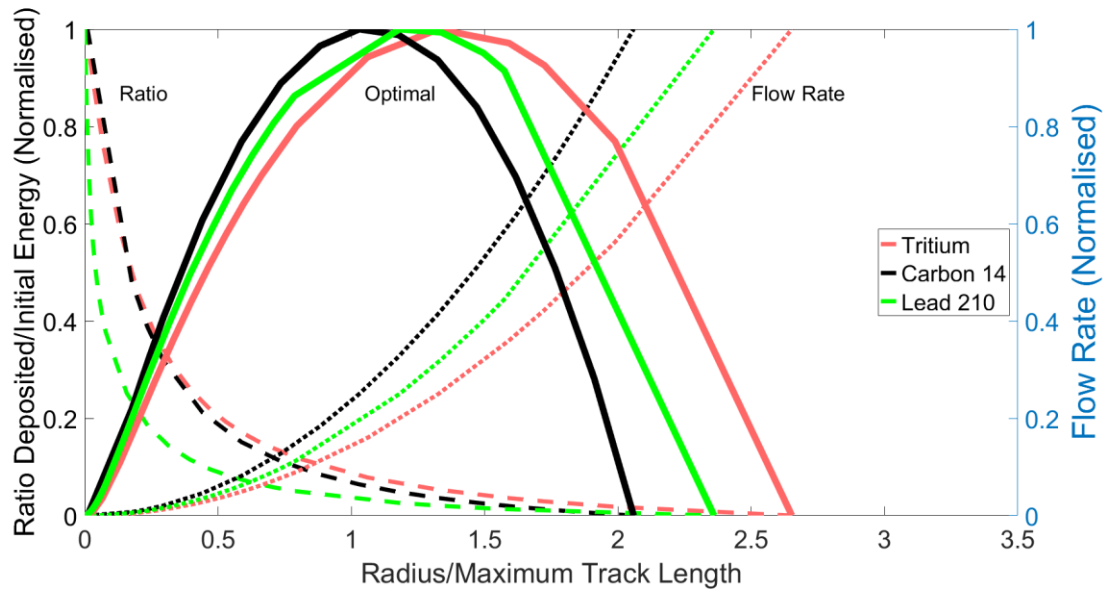
when changing normalising methods.

Figure 10: Results showing the scintillator energy deposition/initial ratio, flow rate and their optimal from multiplication. The scintillator ratio data is the 3D square packing, the efficiency ratio and flow rate data was processed before multiplication. The thick dashed line is the ratio i.e. efficiency, the thin dashed line is the flow rate and the solid line is the optimal value.

4. Conclusions

The Geant4 simulation results show that for the 2D heterogeneous scintillators there is an optimal particle radius whereby the heterogeneous scintillator has a higher efficiency than a single crystal. For the three beta radionuclides examined using the Geant4 simulations (tritium, carbon 14 and lead 210), the maximum increase in efficiency was c.a. 20% when compared with a single crystal. It has been shown that it is possible to approximately predict the optimal radius by using the maximum track length and maximum geometric track length of the beta particle spectrum in water. For the 3D packed arrangements it has been shown that efficiency is inversely proportional to the radius, which is in agreement with the conclusions of Tan and DeVol (Tan and DeVol, 2003). However, it has been further shown that practical considerations based on the flow rate through a 3D packed flow cell show that whilst it is possible to have a high detection efficiency for a static flow or constant concentration using small particle radii, there is a limit to how small the particles can be before transient counting becomes inaccurate.

The experimental results, which confirm the 2D simulations, show that a layer of heterogeneous scintillator has a higher efficiency than a single crystal. The particle size results show that a mortar and pestle is a simple but effective approach to producing a particulate scintillator. Furthermore, PDMS provides a cheap and flexible substrate. It is anticipated that these 2D structures can be layered in such a manner as to be able to produce a flow cell with increased detection efficiency over single crystal layers, with reduced resistance to flow over 3D heterogeneous structures making them potentially an ideal detector for monitoring transient contamination levels.

5. Acknowledgements

6. References

Alton, T., Monk, S., Cheneler, D., 2017. Beta particle energy spectra shift due to self-attenuating effects in environmental sources. J. Nucl. Eng. Technol. 49, 1483–1488. doi:https://doi.org/10.1016/j.net.2017.05.001

Birks, J.B., 2013. The Theory and Practice of Scintillation Counting: International Series of Monographs in Electronics and Instrumentation. Elsevier.

Carman, P.C., 1937. Fluid Flow Through Granular Beds. Inst. Chem. Eng. 75, S32–S48.

Center for Radiation Protection Knowledge, 2015. Rad Toolbox v. 3.0.0.

Corning, D., 2017. SYLGARD 184 SILICONE ELASTOMER KIT [WWW Document]. URL http://www.dowcorning.com/applications/search/products/Details.aspx?prod=010642 91&type=PROD&country=GBR (accessed 8.12.17).

DeVol, T.A., Fjeld, R.A., 1995. Development of an On-line Scintillation Flow-Cell Detection

System with Pulse Shape Discrimination for Quantification of Actinides. IEEE Trans.

Nucl. Sci. 42, 959–963.

Dujardin, C., Amans, D., Belsky, A., Chaput, F., Ledoux, G., Pillonnet, A., 2010. Luminescence

And Scintillation Properties At The Nanoscale. IEEE Trans. Nucl. Sci. 57, 1348–1354.

Elmer, P., 2017. TRI-CARB 4910TR Liquid Scintillation Counter [WWW Document]. URL

https://www.perkinelmer.com/lab-solutions/resources/docs/SPC_Tri-Carb_4910TR.pdf

(accessed 8.20.17).

Gobain, S., 2017. NaI(Tl) and Polyscin NaI(Tl) Sodium Iodide Scintillation Material [WWW

Document]. URL http://www.crystals.saint-

gobain.com/sites/imdf.crystals.com/files/documents/sodium-iodide-material-data-

sheet.pdf (accessed 8.20.17).

Incerti, S., Baldacchino, G., Bernal, M., Capra, R., Champion, C., Francis, Z., Gueye, P.,

Mantero, A., Mascialino, B., Moretto, P., Nieminen, P., Villagrasa, C., Zacharatou, C.,

2010. The Geant4-DNA Project. Int. J. Model. Simulation, Sci. Comput. 1, 157–178.

doi:10.1142/S1793962310000122

J Allison et al, 2006. Geant4 Developments and Applications. Nucl. Sci. IEEE Trans. 53, 270–

278. doi:10.1109/TNS.2006.869826

Kawano, T., Ohashi, H., Hamada, Y., Jamsranjav, E., 2014. Shielding Effect On Tritium Water

Monitoring System Based On CaF2 Flow-Cell Detector. Nucl. Sci. Tech. 25, S010401-3.

Kawano, T., Uda, T., Yamamoto, T., Ohashi, H., 2011. Tritium Water Monitoring System

Based on CaF2 Flow-Cell Detector. Fusion Sci. Technol. 60, 952–955.

Knoll, G.F., 2010. Radiation detection and measurement. John Wiley & Sons.

Materials, H., 2017. Radiation Detection Materials [WWW Document]. URL

http://www.hellma-materials.com/html/seiten/output_adb_file.php?id=63 (accessed

8.20.17).

McCabe, W.L., Smith, J.C., Harriot, P., 2005. Unit Operations of Chemical Engineering, 7th

ed. McGraw-Hill, New York.

Ritter, B., Krahl, T., Rurack, K., Kemnitz, E., 2014. Nanoscale CaF2 doped with Eu3+ and Tb3+

through fluorolytic sol-gel synthesis. J. Mater. Chem. C 2, 8607–8613.

doi:10.1039/c4tc01073f

Sensl, 2017. C Series Datasheet [WWW Document]. URL http://sensl.com/request-c-series-

ds/ (accessed 8.20.17).

Shirahashi, K., Izawa, G., Murano, Y., Muramastu, Y., Yoshihara, K., 1984. Radio-Liquid

Chromatogrphy for Tritium Labelled Organic Compounds Using CaF2/Eu/ Scintillator. J.

Radioanal. Nucl. Chem. 86, 1–9.

T. Kawano H. Ohashi, Y.H., Jamsranjav, E., 2015. Comparative Testing of Various Flow-Cell

Detectors Fabricated Using CaF2 Solid Scintillator. Fusion Sci. Technol. 67, 404–407.

Tan, H., DeVol, T.A., 2003. Monte Carlo Modeling of Heterogeneous Scintillation Flow-Cell

Detectors. Nucl. Instruments Methods Phys. Res. Sect. A Accel. Spectrometers, Detect.

Assoc. Equip. 515, 624–633.

Tony F Chan, Gene H Golub, R.J.L., 1983. Algorithms for Computing the Sample Variance:

Analysis and Recommendations. Am. Statiastician 37, 242–247.

Welford, B.P., 1962. Note on a Method for Calculating Corrected Sums of Squares and

Products. Technometrics 4, 419–420.